

---

This manuscript is a non-peer reviewed preprint submitted to EarthArXiv for public posting. It will be shortly submitted to a scientific journal for peer-review and potential publication. As a function of the peer-review process that this manuscript will undergo, its structure and content may change.

---

# 1 Multi-satellite data depicts record-breaking methane leak from a well 2 blowout

3 Luis Guanter<sup>1,2\*</sup>, Javier Roger<sup>1</sup>, Shubham Sharma<sup>3</sup>, Adriana Valverde<sup>1</sup>, Itziar Irakulis-  
4 Loitxate<sup>4,1</sup>, Javier Gorroño<sup>1</sup>, Xin Zhang<sup>3</sup>, Berend J. Schuit<sup>3,5</sup>, Joannes D. Maasakkers<sup>3</sup>,  
5 Ilse Aben<sup>3</sup>, Alexis Groshenry<sup>6</sup>, Antoine Benoit<sup>6</sup>, Quentin Peyle<sup>6</sup>, Daniel Zavala-Araiza<sup>2</sup>

6 <sup>1</sup>*Research Institute of Water and Environmental Engineering (IIAMA), Universitat Politècnica de*  
7 *València, Spain.*

8 <sup>2</sup>*Environmental Defense Fund, Amsterdam, Netherlands*

9 <sup>3</sup>*SRON Netherlands Institute for Space Research, Leiden, Netherlands*

10 <sup>4</sup>*International Methane Emissions Observatory, United Nations Environment Programme, Paris,*  
11 *France*

12 <sup>5</sup>*GHGSat Inc., Montreal, Canada*

13 <sup>6</sup>*Kayrros, Paris, France*

14 \*To whom correspondence should be addressed; E-mail: lguanter@fis.upv.es

15 **Accidental blowouts in oil and gas wells can result in large and prolonged methane**  
16 **emissions, which are often unreported when happening in remote places. We use**  
17 **satellites to document a massive methane leak from a well blowout in Kazakhstan’s**  
18 **Karaturun East oil field in 2023. The 205-day event resulted in a total of 128±36 kt**  
19 **of methane being released, surpassing the total emissions from all previously re-**  
20 **ported accidents.**

21 Human-induced methane emissions are responsible for about 30% of the global  
22 warming since the pre-industrial period<sup>1</sup>. The oil and gas industry accounts for a large  
23 share of those emissions<sup>2</sup>. However, the mitigation of oil and gas emissions has been  
24 found to be technically feasible and cost-effective<sup>3</sup>, in particular in the case of high-  
25 emitting point sources, also known as super-emitters<sup>4</sup>. Methane super-emitters in the oil  
26 and gas industry are usually linked to unexpected infrastructure failures, such as blowouts  
27 during drilling, completion, or production activities in oil and gas wells. Well blowouts  
28 result in uncontrolled releases of substantial amounts of natural gas, which consists pri-  
29 marily of methane. These accidents often occur in remote areas and are episodic, which  
30 complicates the acquisition of surface and airborne measurements for a proper documen-  
31 tation of the associated gas emissions.

32 A growing constellation of methane-sensitive satellites is now improving our ability  
33 to detect and monitor large methane leaks around the planet. The Sentinel-5P/TROPOMI  
34 mission and a number of high spatial resolution missions are the key assets in this constel-  
35 lation. TROPOMI provides a systematic daily global surveillance of the largest methane  
36 emissions since 2018<sup>5,6</sup>. In contrast, the high-resolution missions have a sparse spatio-

37 temporal sampling as compared with TROPOMI, but scan the Earth at a much higher  
38 spatial resolution, which enables the detection of smaller plumes and the attribution of  
39 those to facility-level sources. Among these high-resolution missions we find the GHGSat  
40 private constellation<sup>7;8</sup>, specifically designed for methane and carbon dioxide mapping at  
41 25–50 m resolution, the EnMAP, PRISMA and EMIT scientific missions, which also have  
42 a relatively high sensitivity to methane<sup>9–11</sup>, and the Sentinel-2 and Landsat multispectral  
43 radiometers, with a lower sensitivity to methane but a frequent global coverage<sup>12</sup>. There  
44 are examples of the potential of those satellites to document methane emissions from  
45 well blowouts: Thompson et al. conducted the first detection of an individual methane  
46 plume with observations of the Aliso Canyon event (Los Angeles, USA) by the Hyperion  
47 high-resolution spectroscopy demonstration mission<sup>13</sup>; Pandey et al. used one TROPOMI  
48 overpass to estimate the emissions caused by a shale gas well blowout in Ohio (USA)<sup>14</sup>;  
49 Maasackers et al. used six TROPOMI overpasses and gas flaring data from the VIIRS  
50 satellite instrument to estimate emissions from a natural gas well blowout in Louisiana  
51 (USA)<sup>15</sup>; Cusworth et al. combined observations from TROPOMI, GHGSat and PRISMA  
52 (four observations in total) to characterise the emissions from a 20-day leak event due to  
53 a gas well blowout in the Eagle Ford Shale (USA)<sup>16</sup>. All these well-documented blowouts  
54 happened in the USA, at sites relatively accessible to well operators and mitigation teams.

55 [Figure 1 about here.]

56 In this work, we have generated a dense time series of more than hundred satellite  
57 observations to document a massive methane emission event triggered by a well blowout  
58 at the Karaturun East oil field in Kazakhstan’s Mangistau region. According to media  
59 reports, the well blowout and subsequent fire happened on the morning of 9 June 2023  
60 during exploration works at well 303<sup>17</sup> (Fig. 1a). The fire destroyed different pieces of  
61 safety equipment, leading to a loss of well control and a 10-m high fire blaze. Days  
62 later, a 15-m wide crater was formed by the collapse of rocks around the wellhead, which  
63 prevented an early seal of the well. The first attempt to halt the flow of gas consisted  
64 of pumping thousands of tons of water through two injection holes between 13 October  
65 and 20 November. This action mitigated the gas leak, but did not completely resolve it.  
66 The flow of gas and the fire could finally be stopped on 25 December 2023 by injecting  
67 heavy drilling mud via a special-purpose probe, which connected with the wellbore of the  
68 accident well at a depth of about 1000 m<sup>18</sup>.

69 Satellites are the only means to document the methane emissions following this  
70 blowout. The leak was first detected in TROPOMI daily global methane concentration  
71 data<sup>17</sup> (Fig. S1). The exact location and date of the blowout could be confirmed with  
72 data from the Sentinel-2 multispectral radiometer, which flew over the site hours after the  
73 accident. The evolution of the leak was then monitored with TROPOMI and a range of

74 high-resolution missions (including PRISMA, EnMAP, EMIT, GHGSat and the Sentinel-  
75 2 and Landsat-8/9 multispectral radiometers), some of which were specifically tasked  
76 to acquire data over the site. Extremely large methane plumes were detected during  
77 the entire time series (Fig. 1b-e). The satellite data were processed with state-of-the-art  
78 algorithms for the detection and quantification of methane plumes from space, optimised  
79 for the particular plume intensities and site characteristics of this event (Methods).

80 We detected methane plumes from the site 115 times between 9 June and 25 De-  
81 cember 2023. After quality screening of all the detected plumes, we retained 48 for the  
82 quantification of emission rates (Methods and Fig. 2). We obtained flux rates between  
83  $3.6 \pm 1.3$  and  $63 \pm 42$  t/h, with typical values between 20 and 50 t/h (Fig. 2a, Supplemen-  
84 tary Fig. S2, and Supplementary Tables S1 and S2). The most substantial emission rates  
85 occurred in the weeks following the blowout (Fig. 2a). Plume intensity gradually decreased  
86 over time until the leak repair on 25 December. Notably, a relatively large plume ( $12 \pm 3$  t/h)  
87 was detected by GHGSat on 25 December, which suggests that the satellite flew over the  
88 site shortly before the final repair action on the same day. Three subsequent observations  
89 on 1, 12 and 14 January 2024 confirmed the definitive cessation of the leak.

90 [Figure 2 about here.]

91 We utilized a time series of fire radiative power derived from the VIIRS FIRMS satel-  
92 lite product to track the fire intensity during the event (Methods). Additionally, we used ob-  
93 servations from high resolution satellites to detect (albeit not quantify) fire at the site. We  
94 found that the strongest fire occurred immediately after the well blowout, with a sustained  
95 relatively high intensity for about 20 days (Fig. 2b). Subsequently, fire activity persisted  
96 throughout the event, as indicated by the active fire detections from the high resolution  
97 satellites. The fire intensity in this event is actually substantially lower than that of strong  
98 flares in oil and gas installations, and also than the intensity of the fires measured during  
99 the Louisiana 2019 event<sup>15</sup> (Supplementary Fig. S3). The relatively low intensity of the  
100 fire at the Karaturun East site would indicate that only a small fraction of the gas outflow  
101 was flared.

102 To give context to the magnitude of the methane plumes detected during the en-  
103 tire Karaturun East leak, the majority of plumes identified in this event exceed 10 t/h and  
104 are comparable to the largest individual plumes detected using global TROPOMI data  
105 worldwide<sup>5,6</sup>. We obtain an estimate of  $128 \pm 36$  kt for the total amount of methane re-  
106 leased to the atmosphere during the event (Methods). This is substantially larger than  
107 the total emission of 97 kt reported for the outstanding 2015 Aliso Canyon blowout, which  
108 is considered the largest methane leak from regular oil and gas operations documented  
109 to date. The total emission from the Karaturun event is also considerably greater than

110 that estimated for the massive releases from the Ohio 2018<sup>14</sup> and the Louisiana 2019<sup>15</sup>  
111 blowout events, for which  $60 \pm 15$  kt and 21–63 kt were estimated, respectively (Fig. 2c).  
112 Only the sabotage of the Nord Stream 1 and 2 subsea twin pipelines in the Baltic Sea on  
113 26 September 2022, for which a total of 420–490 kt has been estimated<sup>19</sup>, may have led  
114 to greater emissions than the Karaturun 2023 blowout event.

115 Our results show that the 2023 well blowout in Kazakhstan’s Karaturun East oil field  
116 has likely caused the largest methane emission from an infrastructure accident ever doc-  
117 umented. The detection and quantification of this leak has only been possible because  
118 of the recent availability of methane-sensitive satellites. It is unknown how many of such  
119 large methane leaks from oil and gas infrastructure failures may have occurred in the last  
120 decades around the world, and how this may have led to underestimated emission inven-  
121 tories. The new era of methane monitoring from space, boosted by international initiatives  
122 such as the Methane Alert and Response System (MARS)<sup>20</sup> implemented by the United  
123 Nations Environment Programme, will be crucial for the detection and quantification of  
124 large methane leaks around the world.

## 125 **Methods**

### 126 *Satellite data*

127 We generated a dense time series of methane observations over the Karaturun East  
128 site using TROPOMI and high-resolution satellite missions. The latter included observa-  
129 tions from the GHGSat private satellite constellation, which offers the highest sensitivity to  
130 methane for this type of high-emitting point source, and from the public hyperspectral mis-  
131 sions EnMAP (German Aerospace Agency, Germany), PRISMA (Italian Space Agency,  
132 Italy) and EMIT (NASA Jet Propulsion Laboratory, USA), which share a relatively similar  
133 configuration, a medium-high sensitivity to methane, and an open data policy. Acquisi-  
134 tions from the less sensitive Sentinel-2 and Landsat multispectral radiometers were also  
135 used for plume detection. A total of 115 plumes were detected between 9 June and 25  
136 December 2023 (26 from TROPOMI and 89 from the high resolution satellites). After  
137 quality control, 48 of those plumes (15 from TROPOMI and 33 from the high resolution  
138 satellites) were retained for the quantification of emissions (Supplementary Figure S2).

139 Satellites were also used to monitor fire activity at the site. Fire radiative power data  
140 from the Fire Information for Resource Management System (FIRMS) based on VIIRS  
141 data were used to assess the evolution of fire intensity. In addition, the observations from  
142 the high resolution satellites from which we derived methane plumes were also utilised to  
143 detect (but not quantify) smaller active fires at the site.

### 144 *Quantification of methane plumes with high spatial resolution satellites*

145 Consolidated processing algorithms were used to infer emission rates from the high  
146 spatial resolution missions.

147 For the retrieval of methane plume information from EnMAP, PRISMA and EMIT  
148 data, which are the bulk of our high-resolution dataset, we adapted the widely-used  
149 matched-filter approach to deal with the large plumes and high methane concentration  
150 values found during the Karaturun East leak. This included the implementation of a log-  
151 normal version of the matched filter and the removal of plume pixels when calculating the  
152 statistics needed for the matched-filter, as described in Pei et al.<sup>21</sup>. The  $\Delta XCH_4$  maps  
153 obtained with this retrieval were screened for quality (cloud-free, no retrieval artifacts, no  
154 substantial fractions of the plume lying outside the image area). The selected high-quality  
155 observations were used for the subsequent flux rate estimation. We manually delineated  
156 the plumes and calculated the integrated methane enhancement (IME), which is the total  
157 mass of methane contained in the plume. The IME values were converted into flux rate  
158 estimates using the IME-based model<sup>22</sup>, which relates the IME, the plume length, and an  
159 effective wind speed parameter ( $U_{\text{eff}}$ ) to the flux rate. For  $U_{\text{eff}}$ , we used empirical linear  
160 models linking  $U_{\text{eff}}$  with 10-m wind speed data ( $U_{10}$ ). These models were specifically de-  
161 rived for the typical  $\Delta XCH_4$  retrieval precision and plume length estimated for this event  
162 (simulated plumes are 5-10 km long). One common  $U_{\text{eff}} - U_{10}$  model was used for En-  
163 MAP and PRISMA, which share the same 30-m resolution and retrieval precision, and a  
164 second one was derived for EMIT in order to account for its 60 m pixels (Supplementary  
165 Fig. S4). Uncertainties in flux rate estimates were derived assuming a 50% uncertainty in  
166 the input wind speed data, which is consistent with previous studies.

167 In the case of GHGSat, the physically-based methane concentration retrieval de-  
168 scribed in Jervis et al.<sup>8</sup> was applied. The performance of GHGSat for the detection and  
169 quantification of methane emissions from oil and gas infrastructure has been extensively  
170 tested during operations in the last years<sup>7</sup>.

171 Finally, in the case of the multispectral missions (Sentinel-2 and Landsat), we have  
172 followed the approach described in Gorroño et al.<sup>12</sup>. This consists of a two-step process-  
173 ing scheme, in which  $\Delta XCH_4$  maps are first derived with a multi-band and multi-pass re-  
174 trieval, and the flux rates are subsequently estimated using the IME-based method. Since  
175 the sensitivity to methane of the multispectral missions is lower than that of GHGSat and  
176 the hyperspectral missions, data from Sentinel-2 and Landsat were mostly used to detect  
177 methane plumes during the event. Thanks to their systematic acquisitions and combined  
178 revisit time of 2-3 days, more than 70 methane plumes could be detected with Sentinel-2  
179 and Landsat. However, only 5 of them, acquired under optimal observation conditions,  
180 were included in the list of 48 plumes used for quantification.

181 Our processing chain to convert radiance to flux rates ( $\Delta XCH_4$  retrieval, plume seg-

182 mentation, IME-based flux rate estimation) has been validated with controlled methane  
183 release tests for all the previous instruments<sup>23</sup>. Since those controlled-release tests were  
184 made for plumes weaker than the ones detected in this event, we also used end-to-end  
185 simulations to test our ability to quantify flux rates for the large plumes and particular con-  
186 ditions of the Karaturun East site. Real top-of-atmosphere radiance data acquired during  
187 the event were used as input for the simulations, so the particular acquisitions conditions  
188 (atmospheric state, illumination angles, potential water vapour and smoke co-emissions  
189 ...) at the site were properly represented. This end-to-end simulation approach has al-  
190 ready been used with hyperspectral and multispectral data<sup>9,12</sup>. We did the simulations for  
191 PRISMA observations of methane plumes over the Karaturun East site within a 5–50 t/h  
192 emission range. The results show that our processing is able to produce reliable flux  
193 estimates for that entire flux rate range (Supplementary Fig. S5).

194 Those simulations confirm the robustness of our methane retrieval and quantification  
195 methods for the particular conditions of the Karaturun East event. In addition, it must be  
196 remarked that we do not find any distortion of our  $\Delta XCH_4$  maps with the water vapour and  
197 smoke being potentially co-emitted by the source (Supplementary Fig. S6). We verified  
198 this by generating water vapour anomaly maps using a similar retrieval method as the  
199 one we use for methane. The resulting water vapour maps show the expected turbulence  
200 patterns, but no water vapour plume superposed to the methane plumes. Also, we do not  
201 detect any smoke signal in the 2300 nm spectral window used for the methane retrievals,  
202 indicating that the smoke plumes may not have a relevant optical activity in this spectral  
203 range for this event, which has also been found in previous studies<sup>10</sup>.

#### 204 *Quantification of methane plumes with TROPOMI*

205 TROPOMI (aboard Sentinel-5P)<sup>24</sup> observes methane with high precision at a res-  
206 olution of  $5.5 \times 7 \text{ km}^2$ , allowing detection of the plume further downwind. We used the  
207 Weather Research and Forecast (WRF) version 4.1<sup>25</sup> to simulate the enhanced methane  
208 concentrations associated with the blowout at a resolution of  $3 \times 3 \text{ km}^2$  from June to De-  
209 cember 2023. We then compared these modelled concentrations to TROPOMI data in a  
210 Bayesian inversion framework<sup>26</sup> to infer daily emissions rates. To obtain simulated plumes  
211 that best match TROPOMI, we ran WRF using two meteorological boundary conditions  
212 products and four planetary boundary layer physics schemes, and sampled the model  
213 at several timesteps around the TROPOMI overpass. Based on daily inversions with all  
214 model setups, we selected the simulations that gave the lowest posterior observation cost  
215 for each day to be used. We only report quantifications for days with clear plumes and  
216 good matches with simulated plumes based on visual inspection. To estimate uncertainty,  
217 we built an ensemble of inversions by varying critical inversion parameters such as data  
218 filtering and the selected simulation. We conservatively report the 2-standard deviation  
219 range from the ensemble as uncertainty. Details on the TROPOMI quantification approach  
220 are given in the Supplementary Text S1.

## 221 *Quantification of total methane emission*

222 We estimate a total of  $128\pm 36$  kt of methane being released to the atmosphere be-  
223 tween 9 June and 25 December. This amount was calculated through the integration of a  
224 polynomial fitted to the time series of 48 flux rate estimates from the plume data passing  
225 the quality screening. The estimation of the uncertainty associated to the total emission  
226 is the result of propagating the uncertainty from each flux rate estimate through the flux  
227 rate interpolation and curve integration using multivariate Monte Carlo simulations. We  
228 assume a 50% correlation between flux rate errors in order to account for both uncor-  
229 related error components (e.g. plume shape changes) and correlated error components  
230 (e.g. same source area) (Supplementary Fig. S7).

231 We tested an alternative option for the quantification consisting of using only the  
232 most accurate flux rate estimates from GHGSat and the hyperspectral missions (i.e., no  
233 plumes from TROPOMI, Sentinel-2 and Landsat), instead of our choice of using all 48  
234 quality-controlled plumes. From this analysis, we found similar total emission numbers for  
235 the two configurations, but the uncertainty of the total emission was substantially lower  
236 when using all 48 plumes, so we opted for this configuration in the calculation of the total  
237 emission and its uncertainty.

## 238 **List of Supplementary Materials**

- 239 • Text S1
- 240 • Tables S1 and S2
- 241 • Figures S1–S7

## 242 **References**

- 243 1. Dhakal, S. *et al.* Emissions trends and drivers. In Shukla, P. *et al.* (eds.) *Climate*  
244 *Change 2022: Mitigation of Climate Change. Contribution of Working Group III to the*  
245 *Sixth Assessment Report of the Intergovernmental Panel on Climate Change*, book  
246 section 2 (Cambridge University Press, Cambridge, UK and New York, NY, USA).
- 247 2. Saunio, M. *et al.* The global methane budget 2000–2017. *Earth System Science*  
248 *Data* **12**, 1561–1623 (2020).
- 249 3. Ocko, I. *et al.* Acting rapidly to deploy readily available methane mitigation measures  
250 by sector can immediately slow global warming. *Environmental Research Letters* **16**  
251 (2021).



- 252 4. Zavala-Araiza, D. *et al.* Reconciling divergent estimates of oil and gas methane emis-  
253 sions **112**, 15597–15602 (2015).
- 254 5. Lauvaux, T. *et al.* Global assessment of oil and gas methane ultra-emitters. *Science*  
255 **375**, 557–561 (2022).
- 256 6. Schuit, B. J. *et al.* Automated detection and monitoring of methane super-emitters  
257 using satellite data. *Atmospheric Chemistry and Physics* **23**, 9071–9098 (2023).
- 258 7. Varon, D. J. *et al.* Satellite Discovery of Anomalously Large Methane Point Sources  
259 From Oil/Gas Production. *Geophysical Research Letters* **46**, 13507–13516.
- 260 8. Jervis, D. *et al.* The GHGSat-D imaging spectrometer. *Atmospheric Measurement*  
261 *Techniques* **14**, 2127–2140 (2021).
- 262 9. Guanter, L. *et al.* Mapping methane point emissions with the PRISMA spaceborne  
263 imaging spectrometer. *Remote Sensing of Environment* **265**, 112671 (2021).
- 264 10. Roger, J. *et al.* High-resolution methane mapping with the EnMAP satellite imaging  
265 spectroscopy mission. *IEEE Transactions on Geoscience and Remote Sensing* 1–1  
266 (2024).
- 267 11. Thorpe, A. K. *et al.* Attribution of individual methane and carbon dioxide emis-  
268 sion sources using EMIT observations from space. *Science Advances* **9**, eadh2391  
269 (2023).
- 270 12. Gorroño, J., Varon, D. J., Irakulis-Loitxate, I. & Guanter, L. Understanding the potential  
271 of Sentinel-2 for monitoring methane point emissions. *Atmospheric Measurement*  
272 *Techniques* **16**, 89–107 (2023).
- 273 13. Thompson, D. R. *et al.* Space-based remote imaging spectroscopy of the Aliso  
274 Canyon CH<sub>4</sub> superemitter. *Geophysical Research Letters* **43**, 6571–6578 (2016).
- 275 14. Pandey, S. *et al.* Satellite observations reveal extreme methane leakage from a nat-  
276 ural gas well blowout **116**, 26376–26381 (2019).
- 277 15. Maasackers, J. D. *et al.* Reconstructing and quantifying methane emissions from the  
278 full duration of a 38-day natural gas well blowout using space-based observations.  
279 *Remote Sensing of Environment* **270**, 112755 (2022).
- 280 16. Cusworth, D. H. *et al.* Multisatellite imaging of a gas well blowout enables quantifica-  
281 tion of total methane emissions. *Geophysical Research Letters* **48**, e2020GL090864.
- 282 17. Clark, A. & Gizitdinov, N. Scientists Say They've Detected a Huge Methane Leak in  
283 Kazakhstan. *Bloomberg* (2023-08-04).
- 284 18. Afanasiev, V. Kazakh operator halts gas fire at well that has been burning since June.  
285 *Upstream* (2023-12-27).

- 286 19. S. Harris et al. Renewed understanding of atmospheric methane emissions from the  
287 2022 Nord Stream pipeline sabotage (2023). Submitted.
- 288 20. UNEP-IMEO. Methane Alert and Response System (MARS). [https://www.unep.org/explore-topics/energy/what-we-do/methane/](https://www.unep.org/explore-topics/energy/what-we-do/methane/imeo-action/methane-alert-and-response-system-mars)  
289 [imeo-action/methane-alert-and-response-system-mars](https://www.unep.org/explore-topics/energy/what-we-do/methane/imeo-action/methane-alert-and-response-system-mars) (2023). [On-  
290 line; accessed 1-February-2024].  
291
- 292 21. Pei, Z. *et al.* Improving quantification of methane point source emissions from imaging  
293 spectroscopy. *Remote Sensing of Environment* **295**, 113652 (2023).
- 294 22. Varon, D. J. *et al.* Quantifying methane point sources from fine-scale satellite obser-  
295 vations of atmospheric methane plumes. *Atmospheric Measurement Techniques* **11**,  
296 5673–5686 (2018).
- 297 23. Sherwin, E. D. *et al.* Single-blind validation of space-based point-source detection and  
298 quantification of onshore methane emissions. *Scientific Reports* **13**, 3836 (2023).
- 299 24. Lorente, A., Borsdorff, T., Martinez-Velarte, M. C. & Landgraf, J. Accounting for sur-  
300 face reflectance spectral features in tropomi methane retrievals. *Atmospheric Mea-*  
301 *surement Techniques* **16**, 1597–1608 (2023).
- 302 25. Powers, J. *et al.* The weather research and forecasting (wrf) model: Overview, system  
303 efforts, and future directions. *Bulletin of the American Meteorological Society* **98**  
304 (2017).
- 305 26. Jacob, D. J. *et al.* Quantifying methane emissions from the global scale down to point  
306 sources using satellite observations of atmospheric methane. *Atmospheric Chemistry*  
307 *and Physics* **22**, 9617–9646 (2022).
- 308 27. Conley, S. *et al.* Methane emissions from the 2015 Aliso Canyon blowout in Los  
309 Angeles, CA. *Science* **351**, 1317–1320 (2016).

## 310 **Acknowledgments**

311 This research was funded by the European Space Agency through the HiResCH4 project  
312 (contract N.4000134929) and the IMEO Science Studies programme (contracts DTIE22-  
313 EN5036 and DTIE23-EN6386). X.Z. acknowledges funding from the Global Methane  
314 Hub. We are thankful to Jason McKeever and the GHGSat team for the acquisition and  
315 processing of the GHGSat data used in this study. Patrizia Sacco and Ettore Lopinto  
316 (Italian Space Agency, ASI) are thanked for the PRISMA acquisitions, and Nicole Pinnel  
317 (German Aerospace Center, DLR) and Sabine Chabrilat (GFZ German Research Centre  
318 for Geosciences) for the EnMAP acquisitions. We are grateful to Daniel J. Varon for the

319 WRF-LES modelled plumes used in this study. Part of this work was carried out on the  
320 Dutch national e-infrastructure, and we thank SURF ([www.surf.nl](http://www.surf.nl)) for the support in using  
321 the National Supercomputer Snellius. Correspondence and request for materials should  
322 be addressed to L.G.

323 **Competing interests:** The authors declare no competing interests.

324 **List of Figures**

325 1 Site overview and examples of methane plumes detected with satellites. **a**,  
326 Location of the Karaturun East oil field (45.3324°N, 52.3730°E) where the  
327 blowout happened on 9 June 2023, including a view of the active fire at  
328 the site (photo from Mangistau Regional Administration). **b-e**, Sample of  
329 methane plumes detected with the PRISMA, EMIT, EnMAP and GHGSat  
330 satellite sensors on different days. The color scale in the maps represent  
331 methane concentration enhancements above background methane levels  
332 ( $\Delta XCH_4$ ). The emission rate (Q) estimated for each plume is provided on  
333 the top right side of each map panel. . . . . 12

334 2 Quantification of methane emissions and fire intensity from the Karaturun  
335 East 2023 blowout. **a**, Time series of methane emission rates (in metric  
336 tonnes per hour, t/h) derived from the satellite observations which passed  
337 the quality screening (see also Supplementary Fig. S2). The black line and  
338 the shaded area represent the polynomial fit that has been integrated for  
339 the calculation of the total amount of methane released during the event.  
340 The black bars depict all satellite observations from which a plume could  
341 be detected, including those that could not be quantified. **b**, Time series of  
342 fire radiative power derived from the VIIRS FIRMS data product. The black  
343 bars depict all satellite detections of active fire at the site. **c**, Comparison  
344 of the total amount of methane released during the Karaturun East 2023  
345 event with the Aliso Canyon 2015<sup>27</sup>, Ohio 2018<sup>14</sup>, and Louisiana 2019<sup>15</sup>  
346 blowout events also leading to massive methane emissions. . . . . 13

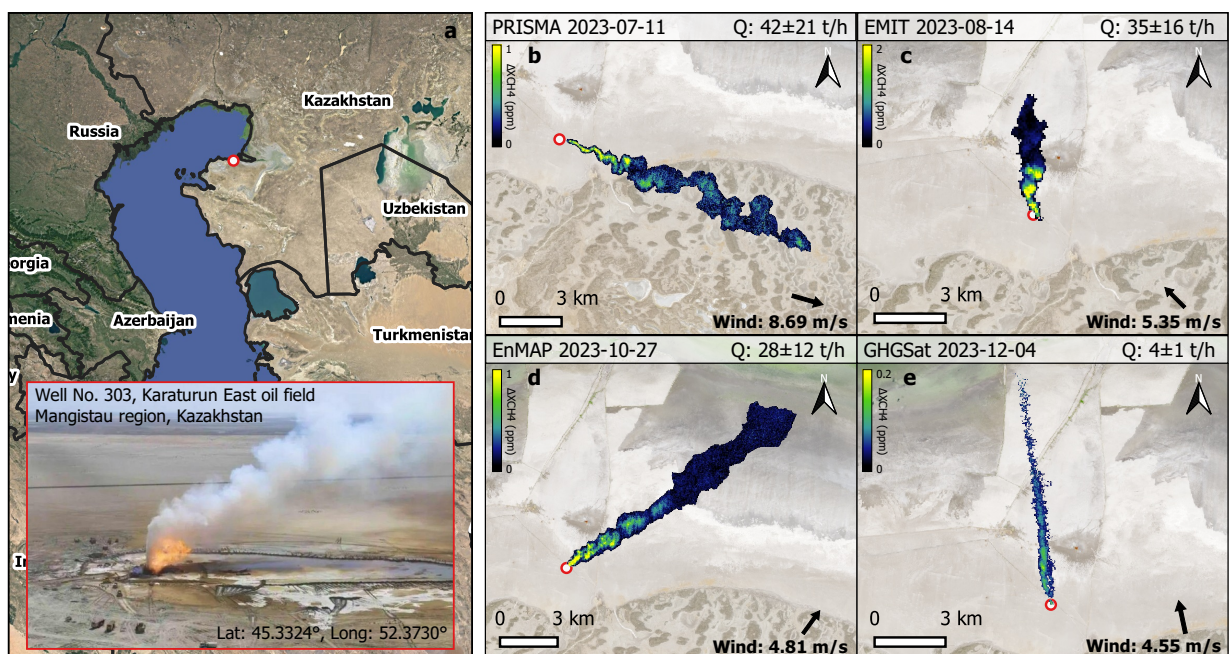


Figure 1: Site overview and examples of methane plumes detected with satellites. **a**, Location of the Karaturun East oil field (45.3324°N, 52.3730°E) where the blowout happened on 9 June 2023, including a view of the active fire at the site (photo from Mangistau Regional Administration). **b-e**, Sample of methane plumes detected with the PRISMA, EMIT, EnMAP and GHGSat satellite sensors on different days. The color scale in the maps represent methane concentration enhancements above background methane levels ( $\Delta XCH_4$ ). The emission rate (Q) estimated for each plume is provided on the top right side of each map panel.

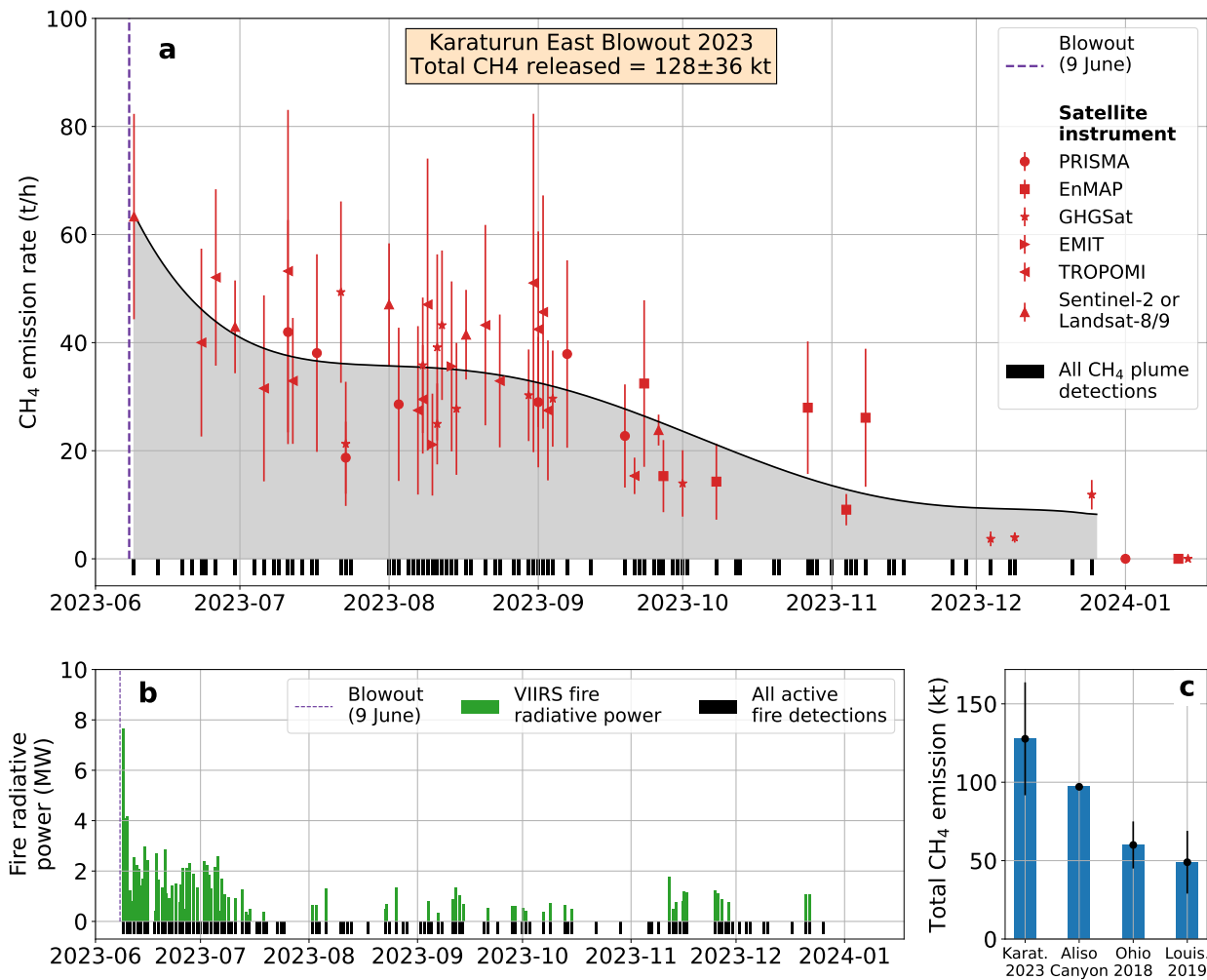


Figure 2: Quantification of methane emissions and fire intensity from the Karaturun East 2023 blowout. **a**, Time series of methane emission rates (in metric tonnes per hour, t/h) derived from the satellite observations which passed the quality screening (see also Supplementary Fig. S2). The black line and the shaded area represent the polynomial fit that has been integrated for the calculation of the total amount of methane released during the event. The black bars depict all satellite observations from which a plume could be detected, including those that could not be quantified. **b**, Time series of fire radiative power derived from the VIIRS FIRMS data product. The black bars depict all satellite detections of active fire at the site. **c**, Comparison of the total amount of methane released during the Karaturun East 2023 event with the Aliso Canyon 2015<sup>27</sup>, Ohio 2018<sup>14</sup>, and Louisiana 2019<sup>15</sup> blowout events also leading to massive methane emissions.

# Supplementary Materials

## Multi-satellite data depicts record-breaking methane leak from a well blowout

Luis Guanter<sup>1,2\*</sup>, Javier Roger<sup>1</sup>, Shubham Sharma<sup>3</sup>, Adriana Valverde<sup>1</sup>, Itziar Irakulis-Loitxate<sup>4,1</sup>, Javier Gorroño<sup>1</sup>, Xin Zhang<sup>3</sup>, Berend J. Schuit<sup>3,5</sup>, Joannes D. Maasakkers<sup>3</sup>, Ilse Aben<sup>3</sup>, Alexis Groshenry<sup>6</sup>, Antoine Benoit<sup>6</sup>, Quentin Peyle<sup>6</sup>, Daniel Zavala-Araiza<sup>2</sup>

<sup>1</sup>Research Institute of Water and Environmental Engineering (IIAMA), Universitat Politècnica de València, Spain.

<sup>2</sup>Environmental Defense Fund, Amsterdam, Netherlands

<sup>3</sup>SRON Netherlands Institute for Space Research, Leiden, Netherlands

<sup>4</sup>International Methane Emissions Observatory, United Nations Environment Programme, Paris, France

<sup>5</sup>GHGSat Inc., Montreal, Canada

<sup>6</sup>Kayrros, Paris, France

\*To whom correspondence should be addressed; E-mail: lguanter@fis.upv.es

## List of Tables

S1	Summary of the emission rates derived from the high-resolution satellite observations passing the quality screening process . . . . .	5
S2	Summary of the emission rates derived from the TROPOMI satellite observations passing the quality screening process . . . . .	6

## List of Figures

S1	Methane column concentration maps for the first observations of the Karaturun 2023 leak by Sentinel-5P/TROPOMI . . . . .	7
S2	Time series of flux rate estimates obtained from the different satellites used in this work	8
S3	Comparison of the fire intensity at the Karaturun 2023 blowout site with that of other gas flaring events . . . . .	9
S4	Empirical $U_{\text{eff}} - U_{10}$ models for IME-based flux rate estimates from EnMAP, PRISMA and EMIT $\Delta X\text{CH}_4$ retrievals . . . . .	10
S5	Verification of $\Delta X\text{CH}_4$ retrievals and flux rate estimates from hyperspectral data with end-to-end simulations . . . . .	11
S6	Assessment of the potential distortion of $\Delta X\text{CH}_4$ retrievals by water vapour and smoke	12
S7	Quantification of the total amount of methane released by the leak . . . . .	13



## Text S1. Quantification of methane plumes with TROPOMI

With daily global coverage, TROPOMI, onboard Sentinel-5P, enables global mapping of methane concentrations at  $5.5 \times 7 \text{ km}^2$  resolution using the shortwave infrared (SWIR) spectrum at  $2.3 \mu\text{m}$ . For this analysis, we use version 02.05.00 of the TROPOMI-CH<sub>4</sub> operational product corrected for stripes<sup>1</sup> with a custom quality filter ( $qa$  value  $\geq 0.4$ , SWIR aerosol optical thickness  $< 0.1$ , SWIR surface albedo  $> 0.05$ , surface classification  $\neq 3$ , and SWIR cloud fraction  $< 0.015$ ).

Methane concentrations are simulated using the Weather Research and Forecast (WRF) version 4.1<sup>2</sup> around the blowout location at a  $3 \times 3 \text{ km}^2$  resolution for an area of  $800 \times 800 \text{ km}^2$  from June 2023 to December 2023. We perform simulations with both 6-hourly National Centre for Environmental Prediction (NCEP)<sup>3</sup> and hourly ERA5<sup>4</sup> meteorological fields. The 6-hourly Copernicus Atmosphere Monitoring Service (CAMS) atmospheric composition forecast data<sup>5</sup> is used to provide the initial and boundary conditions. To infer emissions, the Bayesian cost function  $J$  is minimized to optimize the state vector  $\hat{\mathbf{x}}$ <sup>6</sup>:

$$\hat{\mathbf{x}} = \mathbf{x}_A + \mathbf{S}_A \mathbf{K}^T (\mathbf{K} \mathbf{S}_A \mathbf{K}^T + \mathbf{S}_0^{-1} (\mathbf{y} - \mathbf{K} \mathbf{x}_A)) \quad (1)$$

where  $\mathbf{x}_A$  is the prior state vector, considered 30 t/hr,  $\mathbf{S}_A$  is the prior error covariance matrix assuming 10% uncertainty for the CAMS boundary conditions and 100% uncertainty for the blowout emissions,  $\mathbf{K}$  is the Jacobian matrix, and  $\mathbf{y}$  is the observational vector containing TROPOMI observations. The model output is resampled to match the TROPOMI pixel spatial footprint using TROPOMI averaging kernels. The observations and model are then aggregated to  $0.2^\circ \times 0.2^\circ$  grids to negate model errors.  $\mathbf{S}_0$ , the observational error covariance matrix, is constructed as a diagonal matrix using the standard deviation of the difference between the prior modeled concentrations and TROPOMI observations.

To obtain a simulated plume that best matches the TROPOMI observed plume, we perform an ensemble of WRF simulations using: meteorological fields from either NCEP or ERA5, using four different planetary boundary layer physics options, and sampling the WRF outputs at the TROPOMI overpass time as well as up to 3 hours before and after the overpass time. Preliminary inversions are performed daily using the 56 simulated plumes, and the plumes with the lowest posterior observation cost function are selected. For the final inversion, we optimize the CAMS boundary conditions and the blowout emissions for each day. We only report quantifications for days with clear plumes, no potentially interfering downwind coastal artifacts, and good matches with simulated plumes based on visual inspection. We find that for all reported daily plume quantifications, the averaging kernel value for the blowout is above 0.5, showing the prior value has no significant impact on the estimated emissions. For estimating the uncertainty associated with the quantified emissions, an ensemble of inversions is computed by varying inputs and the assumptions used for the inversion<sup>7</sup>. This includes: increasing and decreasing the prior emissions for the blowout by a factor of 50%; using model outputs

sampled every one hour before and after the overpass hour; using the second best plume match based on observation cost; performing the inversions using different aggregation resolutions ( $0.15^\circ, 0.25^\circ$ ); using TROPOMI data with highest quality flag of 1 ( $qa$  value = 1); using TROPOMI data without filtering for albedo; and following the central limit theorem instead of using mean observational error when aggregating observations, giving us a total of 1728 ensemble members for each day.

	Sensor	Acquisition date	Wind (m/s)	Q (t/h)	Q_err (t/h)
1	Sentinel-2	09/06/2023	3.0	63.3	42.0
2	Landsat 8-9	30/06/2023	2.9	42.9	14.6
3	PRISMA	11/07/2023	8.6	41.9	20.9
4	PRISMA	17/07/2023	7.3	38.0	18.2
5	GHGSAT	22/07/2023	4.6	49.3	16.8
6	GHGSAT	23/07/2023	1.5	21.2	11.4
7	PRISMA	23/07/2023	2.5	18.7	6.7
8	Landsat 8-9	01/08/2023	5.8	47.0	19.1
9	PRISMA	03/08/2023	8.9	28.5	14.1
10	GHGSAT	08/08/2023	4.5	35.8	12.5
11	EMIT	10/08/2023	5.6	21.1	9.4
12	GHGSAT	11/08/2023	2.8	39.1	17.2
13	GHGSAT	11/08/2023	5.6	24.9	7.5
14	GHGSAT	12/08/2023	5.1	43.2	13.8
15	EMIT	14/08/2023	5.3	35.6	15.7
16	GHGSAT	15/08/2023	2.8	27.7	12.2
17	Landsat 8-9	17/08/2023	3.9	41.4	15.4
18	GHGSAT	30/08/2023	6.3	30.2	8.5
19	PRISMA	01/09/2023	3.9	28.9	12.0
20	GHGSAT	04/09/2023	5.6	29.6	8.9
21	PRISMA	07/09/2023	5.7	37.8	17.3
22	PRISMA	19/09/2023	4.0	22.7	9.5
23	ENMAP	23/09/2023	6.9	32.4	15.4
24	Landsat 8-9	26/09/2023	4.9	23.8	9.3
25	ENMAP	27/09/2023	4.7	15.3	6.7
26	GHGSAT	01/10/2023	2.6	13.9	6.1
27	ENMAP	08/10/2023	8.5	14.2	7.0
28	ENMAP	27/10/2023	4.8	27.9	12.2
29	ENMAP	04/11/2023	1.9	9.0	2.9
30	ENMAP	08/11/2023	8.1	26.1	12.8
31	GHGSAT	04/12/2023	4.5	3.6	1.3
32	GHGSAT	09/12/2023	9.7	3.9	0.9
33	GHGSAT	25/12/2023	8.2	11.8	2.7

**Table S1: Summary of the emission rates derived from the high-resolution satellite observations passing the quality screening process.** This quality screening has removed the observations with cloud contamination, retrieval artifacts and plumes for which a substantial part of the tail lied outside the imaged area. Q refers to the flux rate estimated for each plume, and Q\_err to the associated 1- $\sigma$  uncertainty.

	Sensor	Acquisition date	Q (t/h)	Q_err (t/h)
1	TROPOMI	23/06/2023	40.0	17.3
2	TROPOMI	26/06/2023	52.0	16.3
3	TROPOMI	06/07/2023	31.5	18.4
4	TROPOMI	11/07/2023	53.2	29.9
5	TROPOMI	12/07/2023	32.9	14.3
6	TROPOMI	07/08/2023	27.4	12.6
7	TROPOMI	08/08/2023	29.5	12.6
8	TROPOMI	09/08/2023	47.0	23.1
9	TROPOMI	21/08/2023	43.2	20.8
10	TROPOMI	24/08/2023	32.9	17.1
11	TROPOMI	31/08/2023	51.0	31.3
12	TROPOMI	01/09/2023	42.4	29.7
13	TROPOMI	02/09/2023	45.6	21.5
14	TROPOMI	03/09/2023	27.4	17.1
15	TROPOMI	21/09/2023	15.3	3.3

**Table S2: Summary of the emission rates derived from the TROPOMI satellite observations passing the quality screening process.** This quality screening has consisted in the selection of only clear plumes and of good matches with simulated plumes based on visual inspection. Q refers to the flux rate estimated for each plume, and Q\_err to the associated 1- $\sigma$  uncertainty.

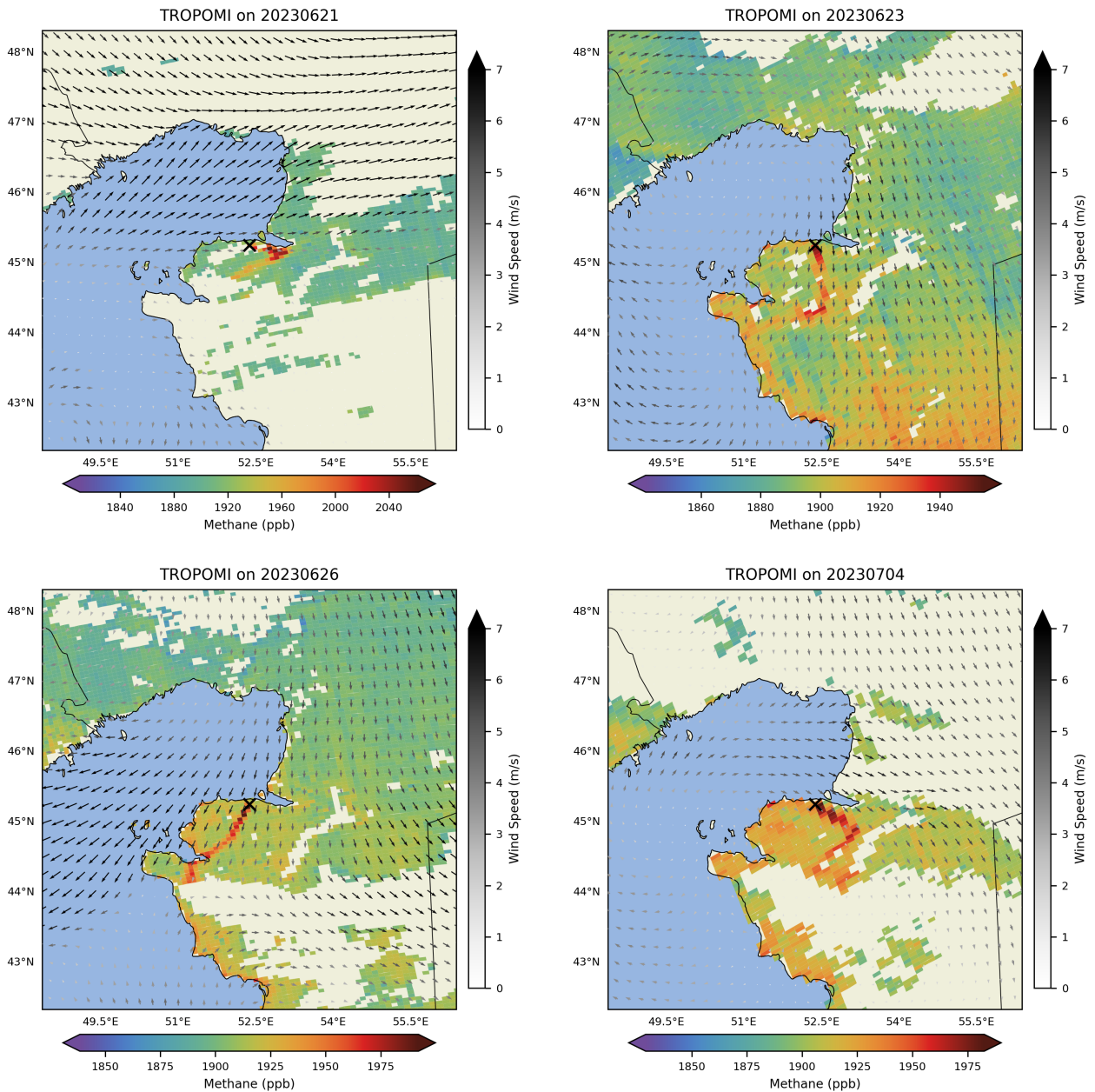


**Figure S1: Methane column concentration maps for the first observations of the Karaturun 2023 leak by Sentinel-5P/TROPOMI.** Data are from the TROPOMI-CH<sub>4</sub> operational product (02.05.00 version). The color scale indicates the total methane column concentration estimated from TROPOMI (as opposed to the concentration enhancement derived from the high resolution data). Arrows indicate wind intensity and direction. TROPOMI data on 21 June and 4 July were not used to quantify emissions as we could not obtain a good match with a modeled plume.

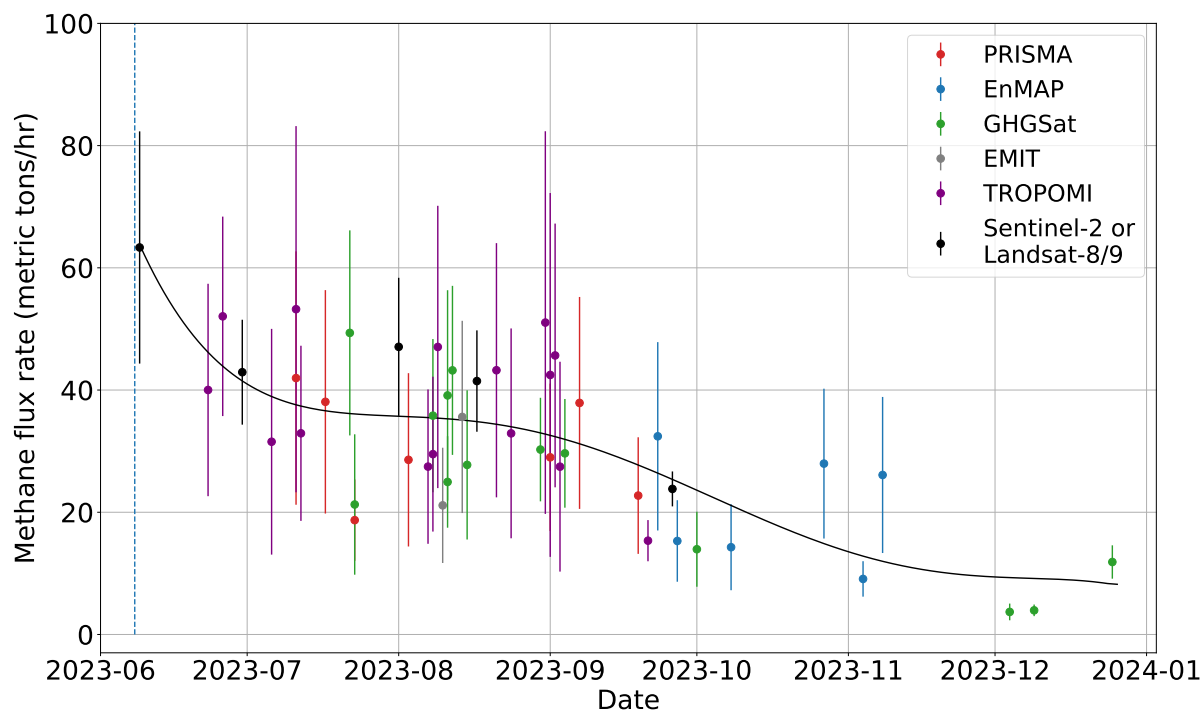
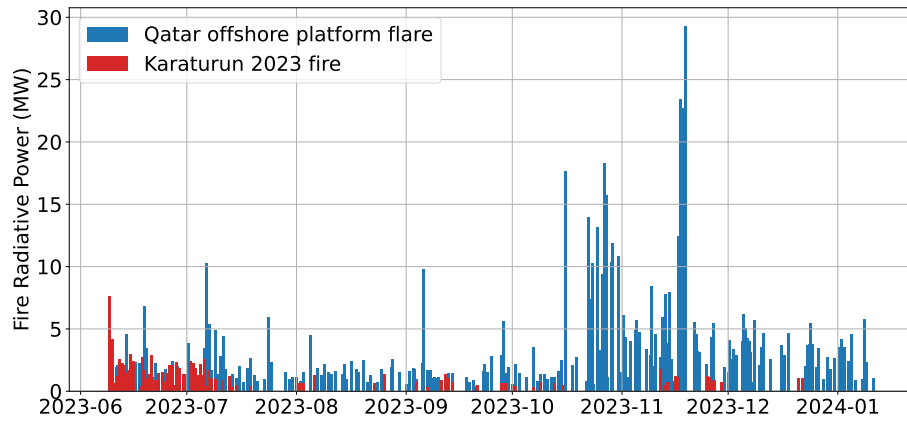
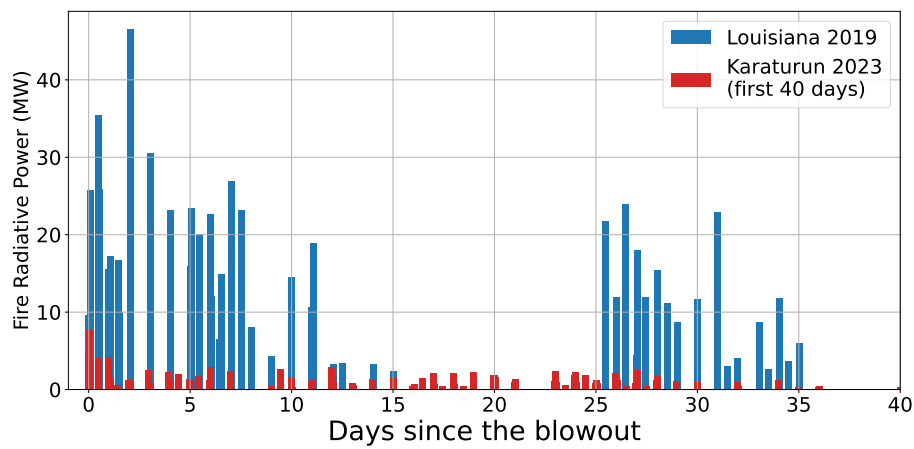


**Figure S2: Time series of flux rate estimates obtained from the different satellites used in this work.** The points represent the flux rate estimates for the 48 plumes retained for quantification after quality screening. This figure offers a more clear representation of the data derived from each satellite as compared with Fig. 2 of the Main Text.



(a)



(b)

**Figure S3: Comparison of the fire intensity at the Karaturun 2023 blowout site with that of other gas flaring events.** (a) Regular flare in an offshore platform in Qatar ( $26.59^{\circ}\text{N}$ ,  $52.00^{\circ}\text{E}$ ). (b) Fire intensity during the Louisiana 2019 event ([Maasackers et al., 2022](#)), where gas burned first at the wellheads for two weeks, and then at a flare pit for 10 days, with a 10-day period in between during which the gas was vented. In both cases, fire intensity is proxied by the fire radiative power variable provided in the VIIRS Fire Information for Resource Management System (FIRMS) product.

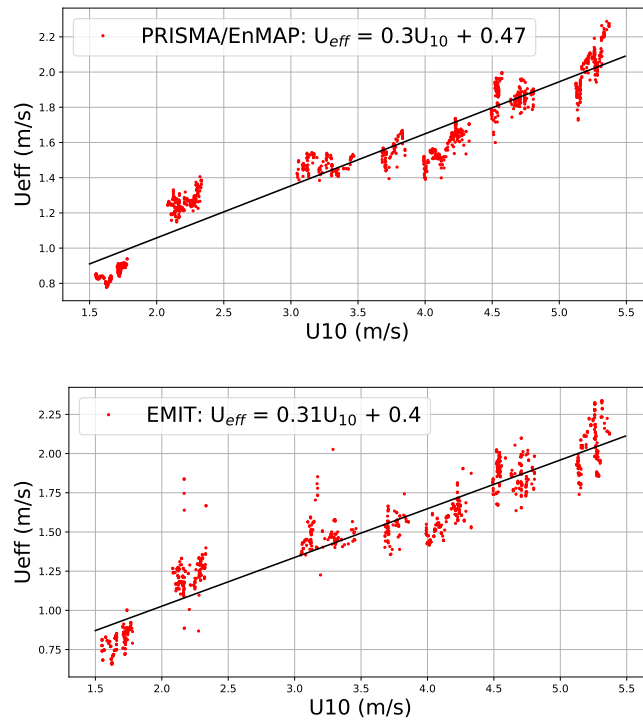


**Figure S4: Empirical  $U_{\text{eff}} - U_{10}$  models for IME-based flux rate estimates from EnMAP, PRISMA and EMIT  $\Delta\text{XCH}_4$  retrievals.** The linear models have been generated using a database of plumes simulated with a WRF-LES modeling approach. The plume simulations cover the flux rate range of 10–90 t/h, and are done for the  $\Delta\text{XCH}_4$  retrieval noise found in the Karaturun East site for those missions. Separate models have been generated for EnMAP-PRISMA and EMIT because of the different spatial sampling (30 m for EnMAP-PRISMA and 60 m for EMIT). Retrieval precision is assumed to be similar for EnMAP and PRISMA.



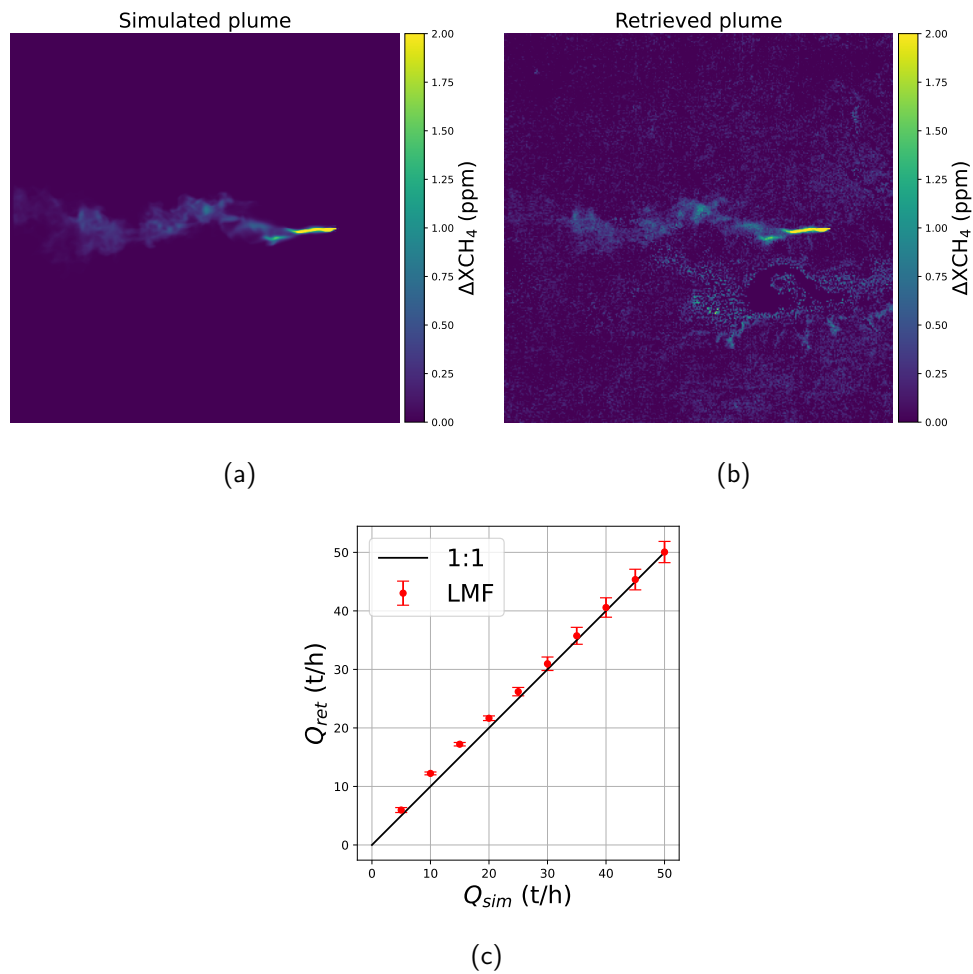


**Figure S5: Verification of  $\Delta XCH_4$  retrievals and flux rate estimates from hyperspectral data with end-to-end simulations.** (a), Simulated methane plume (25 t/h) added to a real PRISMA radiance dataset. (b), Methane plume retrieved from the processing of the resulting PRISMA radiance dataset using the  $\Delta XCH_4$  retrieval scheme implemented for this study. (c), Comparison of the input and estimated flux rates ( $Q_{sim}$  and  $Q_{ret}$ , respectively) from the entire end-to-end simulation process.

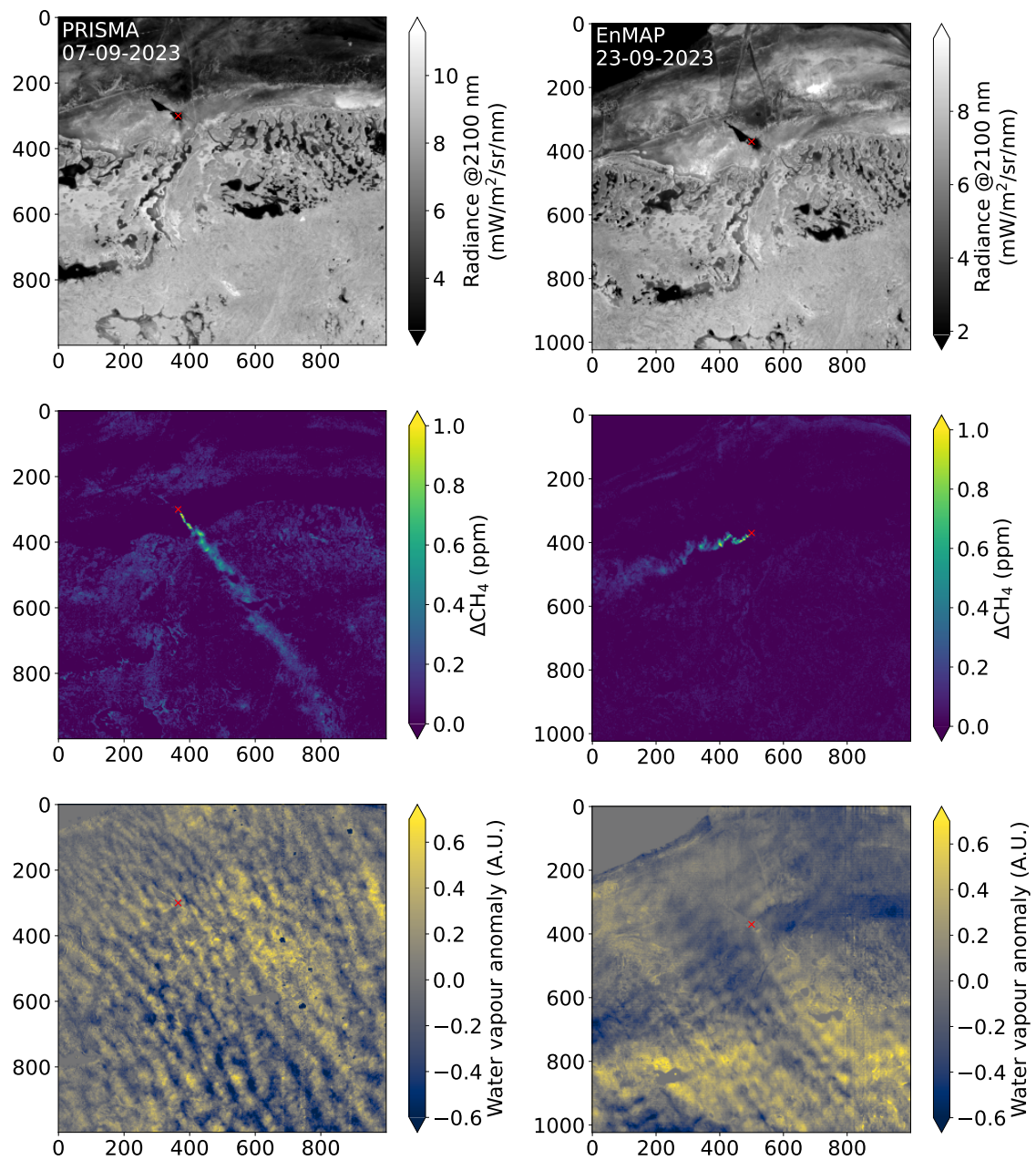
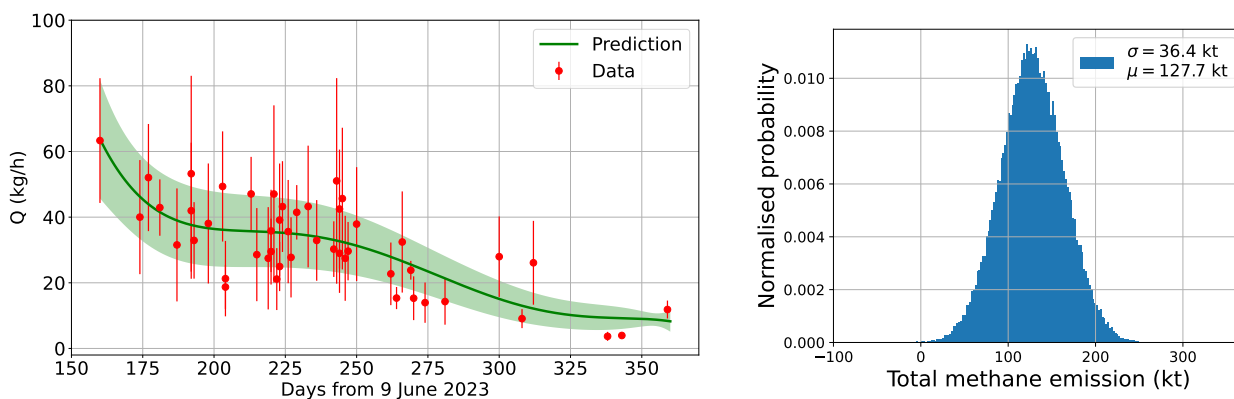
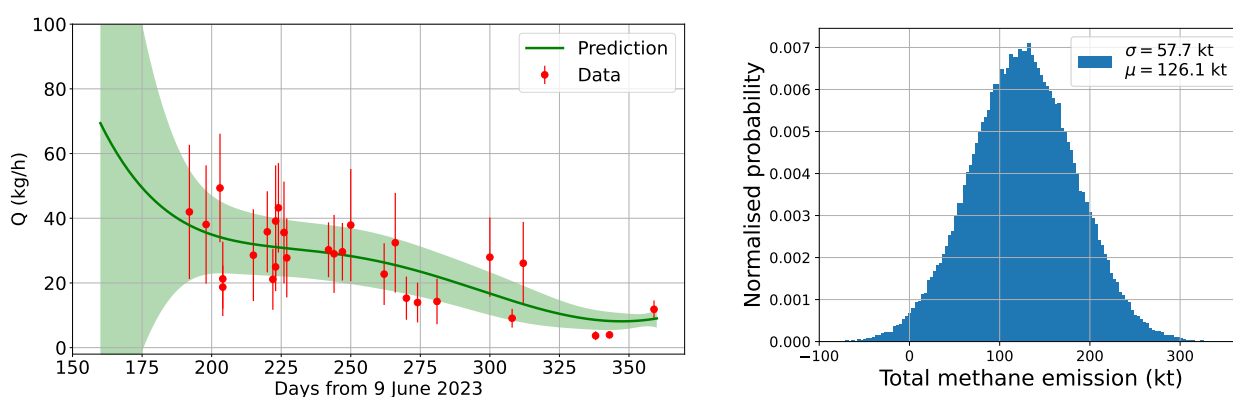


**Figure S6: Assessment of the potential distortion of  $\Delta XCH_4$  retrievals by water vapour and smoke.** Maps of at-sensor radiance at 2100 nm (top row),  $\Delta XCH_4$  (center row), and water vapour concentration anomaly (bottom row) derived from a PRISMA acquisition from 7 September 2023 (left column), and an EnMAP acquisition from 23 September 2023 (right column). No water vapour plume superposed to the methane plume can be observed from the comparison of  $\Delta XCH_4$  and water vapour anomaly maps. Also, no smoke plume can be observed in the 2100 nm radiance maps, which suggests that, in this particular event, smoke has a negligible optical activity on the shortwave infrared window from which  $\Delta XCH_4$  maps are retrieved.



(a) All 48 high-quality plumes used for the total emission quantification (see Fig. 2a and Fig. S2)



(b) Hyperspectral-only plume detections (PRISMA, EnMAP, EMIT, GHGSat)

**Figure S7: Quantification of the total amount of methane released by the leak.** Top row, results from the dataset consisting of the 48 high quality plumes (including TROPOMI as well as hyperspectral and multispectral high-resolution observations) used in this study for the quantification of the leak in this study. Bottom row, results from an alternative hyperspectral-only configuration. The time series on the left hand side depict a polynomial fit of the satellite-based flux rate estimates ( $Q$ ) selected after quality screening. The fitted model is integrated to obtain an estimate of the total leak. The shaded green area corresponds to the uncertainty ( $k=1$ ) of the flux rate fitting. The probability distribution functions on the right hand side show the result of propagating the temporal flux rate together with the uncertainty using multivariate Monte Carlo simulations. An error correlation of 0.5 is assumed for the individual satellite observations. The comparison between the top and bottom row illustrates the fact that the extra observations from TROPOMI and the multispectral missions contribute to decrease the uncertainty range but have a very low impact on the total emission estimate.

## References

1. Borsdorff, T. *et al.* Measuring carbon monoxide with tropomi: First results and a comparison with ecmwf-ifs analysis data. *Geophysical Research Letters* **45**, 2826–2832 (2018). URL <https://agupubs.onlinelibrary.wiley.com/doi/abs/10.1002/2018GL077045>. <https://agupubs.onlinelibrary.wiley.com/doi/pdf/10.1002/2018GL077045>.
2. Powers, J. G. *et al.* The weather research and forecasting model: Overview, system efforts, and future directions. *Bulletin of the American Meteorological Society* **98**, 1717 – 1737 (2017). URL <https://journals.ametsoc.org/view/journals/bams/98/8/bams-d-15-00308.1.xml>.
3. National Centers for Environmental Prediction, National Weather Service, NOAA, U.S. Department of Commerce. Ncep fnl operational model global tropospheric analyses, continuing from july 1999 (2000). URL <https://doi.org/10.5065/D6M043C6>.
4. Hersbach, H. *et al.* The era5 global reanalysis. *Quarterly Journal of the Royal Meteorological Society* **146**, 1999–2049 (2020). URL <https://rmets.onlinelibrary.wiley.com/doi/abs/10.1002/qj.3803>. <https://rmets.onlinelibrary.wiley.com/doi/pdf/10.1002/qj.3803>.
5. N, K. & P, B. Evaluation of copernicus atmosphere monitoring service methane products (2018).
6. Jacob, D. J. *et al.* Satellite observations of atmospheric methane and their value for quantifying methane emissions. *Atmospheric Chemistry and Physics* **16**, 14371–14396 (2016). URL <https://acp.copernicus.org/articles/16/14371/2016/>.
7. Maasackers, J. D. *et al.* Using satellites to uncover large methane emissions from landfills. *Science Advances* **8**, eabn9683 (2022). URL <https://www.science.org/doi/abs/10.1126/sciadv.abn9683>. <https://www.science.org/doi/pdf/10.1126/sciadv.abn9683>.